

UAN: Unified Attention Network for Convolutional Neural Networks

Tony Joseph*, Konstantinos G. Derpanis**, Faisal Z. Qureshi*,
 {*University of Ontario Institute of Technology, **Ryerson University}, Canada
 {tony.joseph, faisal.qureshi}@uoit.ca

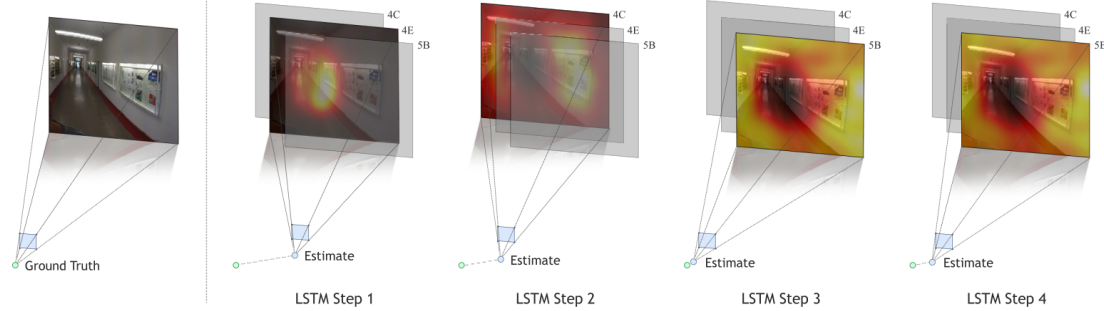


Figure 1: The proposed unified attention network learns “where” to look in, and at “what” level of abstraction. Here, at each timestep, the network selects a single layer—from GoogleNet layers Conv-4C, Conv-4E and Conv-5B—whose feature map is processed via a soft attention mechanism to estimate the position and orientation of the camera.

Abstract

We propose a new architecture that learns to attend to different Convolutional Neural Networks (CNN) layers (i.e., different levels of abstraction) and different spatial locations (i.e., specific layers within a given feature map) in a sequential manner to perform the task at hand. Specifically, at each Recurrent Neural Network (RNN) timestep, a CNN layer is selected and its output is processed by a spatial soft-attention mechanism. We refer to this architecture as the Unified Attention Network (UAN), since it combines the “what” and “where” aspects of attention, i.e., “what” level of abstraction to attend to, and “where” should the network look at. We demonstrate the effectiveness of this approach on two computer vision tasks: (i) image-based camera pose and orientation regression and (ii) indoor scene classification. We evaluate our method on standard benchmarks for camera localization (Cambridge, 7-Scene, and TUM-LSI datasets) and for scene classification (MIT-67 indoor dataset), and show that our method improves upon the results of previous methods. Empirically, we show that combining “what” and “where” aspects of attention improves network performance on both tasks.

1. Introduction

This paper develops a model of computational attention for deep networks. Since 2012, deep learning based ap-

proaches have seen unprecedented success in many computer vision tasks, such as object detection [11], semantic segmentation [10], video tracking [38], motion estimation [13], image generation [26], etc. Most deep networks for computer vision applications share a common structure. In most architectures, the first few layers of the network consists of convolutional layers that are glued together using interleaving layers: activation, maxpool, etc. [25, 23]. Loosely speaking we can refer to this setup as the Convolutional Neural Network (CNN) subnet. One can argue that the success of deep learning for computer vision tasks lie in part on the ability of CNNs to learn powerful image representations from data. The image representation constructed by CNNs are sometimes called *deep features*. These deep features, to a large extent, have displaced the hand-crafted features of old, which predate the wide-spread use of deep learning in computer vision by at least two decades.

It is straightforward to designate the image representations at a particular CNN layer as the deep feature that will be used during subsequent processing. It is also possible to combine image representations at multiple convolutional layers to construct the deep feature. It has been observed that different CNN layers capture information at different levels of abstraction [43]. Layers that are closer to the input capture fine-grained spatially localized structures, say edges and blobs; whereas, layers that are further away from the input capture more abstract information, such as existence of a cat or a dog. To the best of our knowledge, the

decision about which CNN layer(s) provide the deep features is made at design time. In other words, “what” should the network look at—edges and blobs or cats and dogs—is hardwired.

Deep features, especially those that are constructed by convolutional layers, encode spatial information, i.e., a given deep feature layer that picks a cat will also encode the location of this cat. When one is searching for a cat, knowing “where” to look can help. [41] developed an attention mechanism that focuses on different locations in the deep feature¹ over successive steps. This attention mechanism, which we henceforth refer to as *soft attention*, has been applied successfully to the problem of image captioning.

We argue that there is another kind of attention that we can exploit. We call this “what” level of abstraction to attend to. The “what” attention guides a network to pick a CNN layer that outputs deep features containing the most promising information for solving the task at hand. We refer to this kind of attention as *hard attention*, since it makes a hard choice between one of many layers. Empirically, we show later, what others have already demonstrated, that the choice of CNN layer for constructing the deep feature has an effect on the overall task performance.

1.1. Why “what?”

Let us first consider the problem of image-based camera pose regression. We manually selected different CNN layers whose outputs were fed into a soft attention mechanism to regress camera position and orientation (Table 1). The goal of this exercise is to confirm that using different CNN layers gives different results. Let us set the final CNN layer’s² result as the baseline; outputs of the final layers often form the deep feature for subsequent processing. We want to see if selecting a different CNN layer can reduce errors. The results in these tables confirm our intuition. Pose estimation errors decrease when we select the *fifth-last* layer. A similar trend is observed for the Office dataset. It is also interesting to note that the *last* layer yields better results for TUM-LSI dataset. Table 2 shows the results of a similar exercise for the scene classification problem. Here we find that the classification accuracies increase as we select layers other than the *last* layer. This little experiment suggests that always selecting the *last* layer output may not be the best strategy. Furthermore, we argue that the “correct” layer for a particular task depends both on the task and the image over which inference is performed. We will return to this set of experiments later.

¹Or one might say that it selects different layers within the feature map that forms the deep feature.

²GoogLeNet [34] Conv-5B feature.

1.2. Contributions

This work combines the “what” and the “where” aspects of attention. We propose a new network architecture that learns a policy for focusing attention at different CNN layers (i.e., different levels of abstractions) and different spatial locations (within the chosen CNN layer outputs) over successive Long Short-Term Memory (LSTM) steps. Deep features constructed at each LSTM step are subsequently used to solve the task at hand. UAN essentially allows salient task-related information to be selected and integrated in a sequential fashion.

We demonstrate UAN over two computer vision tasks: image-based camera localization and indoor scene classification. We evaluate the proposed architecture over standard benchmarks: (a) Cambridge Landmarks, 7 Scenes, and TU Munich Large-Scale Indoor (TUM-LSI) datasets for camera pose estimation; and (b) MIT-67 indoor scenes for scene classification. Our results suggest that combining “what” with “where” attention yields better results than their respective baselines.

For image-based camera localization we compare our work with previous approaches proposed in [21], [18] and [37] on 7-Scenes, Cambridge Landmarks, and TUM-LSI. The TUM-LSI dataset contains large textureless surfaces and repetitive scene elements that covers over $5,575\text{ m}^2$. Active search or SIFT based approaches are known to perform poorly on this dataset [37]. Our method does well on this dataset, suggesting that the ability to attend to different CNN layers over successive LSTM steps helps. For indoor scene classification, we compare UAN with existing approaches [32] and [9] on MIT-67 indoor scene dataset [30]. Please refer to Sec. 4.2 for a discussion on the different datasets used in this paper.

2. Related Works

Attention and RNNs Attention has been incorporated into CNNs for a variety of computer vision tasks [24, 35, 16]. Ba *et al.* [3, 28] proposed a model for a multiple object recognition in a single input image. At each time step the model probes through the input image to effectively classify multiple objects. The network is trained using reinforcement learning. Attention requires looking at different parts of the inputs one after the other in rapid succession. Recurrent Neural Networks (RNNs) provide a natural way to model a mechanism that can learn a policy for controlling how attention is directed from one portion of the image to the other over successive steps [8]. LSTM networks [12], a variant of Recurrent Neural Networks (RNNs), are designed to accumulate and discard information captured in its hidden states. RNNs, and especially LSTMs, have been used successfully to process sequential data: video processing [7], gaze predictions [29], image captioning [41], etc. Cur-

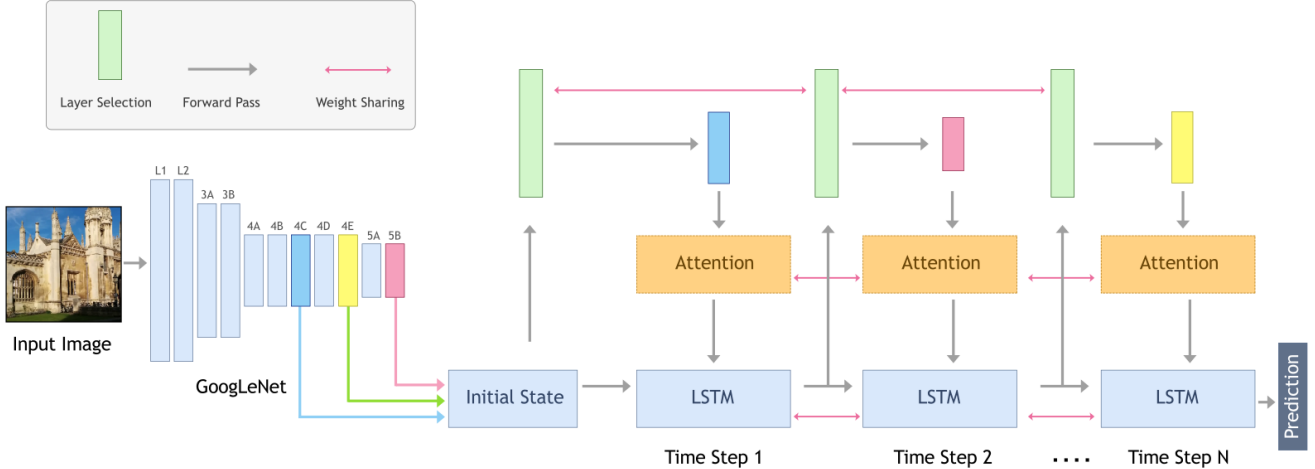


Figure 2: Unified Attention Network.

rent implementations of LSTM closely follow [42]. Compared to Fully Connected LSTM, Shi *et al.* [40] proposed a Convolutional-LSTM (ConvLSTM) that allows for spatial information to be captured in both input-to-state and state-to-state transitions. Veit & Belongie [36] proposed an architecture that selects whether or not information propagates through a given CNN layer during a forward pass.

Image-based camera pose regression Prior to deep learning, SIFT based approaches have been explored for image-based camera localization [2, 31]. Kendall *et al.* [21, 18] proposed PoseNet, an image-based six degree of freedom camera localization method. PoseNet casts camera localization as a regression problem, where camera position and orientation are regressed from the input image. PlanNet [39] deals with the problem of approximate camera localization. It casts camera pose estimation as a classification problem. Work by [37] improves upon PoseNet. It introduces an LSTM-based dimensionality reduction step prior to regression to avoid overfitting. This work improves upon the results posted by PoseNet. Geometric PoseNet [19] also builds upon PoseNet. It uses geometric loss and reprojection error during network training to further improve the localization accuracy. Current state-of-the-art camera localization results are achieved by [5]. This method infers a 3D model of the scene from the training data, and uses it subsequently during training and inference. [4] is another camera localization technique that relies upon learning a 3D model from data. This method is evaluated on 7-Scenes and RelocDB datasets. We compare our approach with schemes in [21], [18], and [19]. All of these schemes treat camera localization as a regression problem. These methods, we believe, provide a sound testing ground for exploring our unified attention network.

Indoor scene classification Some might argue that indoor

scene classification is more challenging than object classification, since decisions about the former often rest upon the number of and the relationship between objects. Broadly speaking, we can divide existing indoor scene classification approaches into two categories; those that rely upon global characteristics vs. those that use local cues. Doersch *et al.* [6] proposed a discriminative variant of the mean-shift algorithm for finding visual elements that can aid in scene classification. Juneja *et al.* [17] learns a parts-model to discover distinct parts of a scene class. Sharif *et al.* [32] proposed a method where deep features from a pre-trained CNN are fed into a Support Vector Machine (SVM) classifier for scene classification. Recently Hayat *et al.* [9] introduced a learnable feature descriptor layer that introduces location and scale invariance directly into CNN. The performance gain, however, of this approach is minimal over Sharif *et al.*'s method on the MIT-67 indoor scenes dataset.

3. Unified Attention Network

UAN comprises of a ConvLSTM, a soft attention mechanism and a hard selection (or a CNN layer selection) mechanism (Fig. 2). We guide the reader to [40] for technical details on ConvLSTM. Below we briefly discuss the soft attention mechanism that we use, and provide technical details for layer selection in Sec. 3.2. The loss functions that we used during training are explained in Sec. 3.3.

3.1. Feature selection using Soft Attention

We adapt the soft attention mechanism from Xu *et al.* [41] for our purposes. At each time step t , the input to the attention layer consists of deep feature (specifically, the feature map) from (the currently selected) CNN layer plus the LSTM hidden state from the previous time step. Specif-

ically, we used a multi-convolutional LSTM modeled after inception module [34]. At each time step, the attention mechanism selects a feature it deems most likely to improve task performance.

3.2. Layer selection using Hard Attention

Layer selection involves the process of selecting a single layer at each time step t . This is a discrete decision. We essentially need a scheme to compute $\arg \max$, an operation that is not differentiable. We use the Gumbel-Max trick, first proposed in [27], to get around this.

Gumbel-Max provides a simple and efficient way to draw samples:

$$z = \text{one_hot}(\arg \max[g_i + \log \pi_i]), \quad (1)$$

where g_1, \dots, g_k are i.i.d. samples drawn from Gumbel(0, 1) distribution, and π_i are unnormalized probabilities. We can construct samples g using the following recipe: (i) Draw sample $u \sim \text{Uniform}(0, 1)$; and (ii) set $g = -\log(-\log(u))$.

During backward computation of gradients, $\arg \max$ is approximated with a *softmax* function [15] as shown below

$$y_i = \frac{\exp\left(\frac{\log(\pi_i) + g_i}{\tau}\right)}{\sum_{j=1}^k \exp\left(\frac{\log(\pi_j) + g_j}{\tau}\right)}. \quad (2)$$

Here k is the number of CNN layers that are considered for selection, $i \in [1, k]$, and τ represents temperature.

At each time step, the hard selection mechanism selects a particular layer i during the forward pass. The attention mechanism seeks to select the layer whose output³ achieves best task performance.

3.3. Training Losses

To ensure that our comparisons are meaningful, and that any differences in the performance of our method to those posted by previous methods are due to our unified attention mechanism, we chose the exact same losses as those used by the previous methods.

Camera pose estimation We use the same regression loss as [21], [20], and [37]:

$$\mathcal{L} = \|\mathbf{x} - \hat{\mathbf{x}}\|_2 + \beta \|\mathbf{q} - \frac{\hat{\mathbf{q}}}{\|\hat{\mathbf{q}}\|}\|_2 \quad (3)$$

where $[\mathbf{x}, \mathbf{q}]^\top$ represent ground truth position \mathbf{x} and orientation \mathbf{q} , and $[\hat{\mathbf{x}}, \hat{\mathbf{q}}]^\top$ denote predicted position $\hat{\mathbf{x}}$ and orientation $\hat{\mathbf{q}}$. Orientations are represented using quaternions. β is a scalar hyperparameter that determines the relative weighting between the positional and orientation errors.

³We have been referring to this output interchangeable as deep features or feature maps.

Scene	Layer 5B	Layer 4E	Layer 4D	Layer 4C
Old Hospital	3.04 m, 4.30°	1.74 m, 4.07°	1.62 m, 4.47°	1.54 m, 4.01°
Office	0.47 m, 7.96°	0.28 m, 7.78°	0.31 m, 7.42°	0.28 m, 7.70°
TUM-LSI	1.15 m, 2.87°	1.34 m, 5.54°	1.36 m, 4.53°	1.45 m, 5.18°

Table 1: Image-based camera localization. Median localization error after spatial soft attention to feature maps from different GoogLeNet layers.

Scene	Layer 5B	Layer 4E	Layer 4D	Layer 4C
Auditorium	38.8	66.6	61.1	61.1
Children Room	27.7	38.8	72.2	50.0
Concert Hall	95.5	90.0	90.0	80.0
Garage	77.7	83.3	88.8	88.8
Laboratory Wet	54.5	86.3	81.8	81.8
Shoe Shop	73.6	73.6	88.9	73.6

Table 2: Indoor scene classification. Mean Accuracy results (%) after spatial soft attention to feature maps from different GoogLeNet layers.

Consistent with prior work, the proposed camera localization network takes an RGB image as input and outputs camera position and orientation $[\mathbf{x} \ \mathbf{q}]^\top$. Camera pose is defined relative to an arbitrary reference frame.

Indoor scene classification We use the standard cross-entropy classification loss consistent with [41] and [34]:

$$\mathcal{L} = -\mathbf{y}_c^\top \log(\hat{\mathbf{y}}_c). \quad (4)$$

Here \mathbf{y}_c is one-hot encoded class label for class c , and $\hat{\mathbf{y}}_c$ is the output of the softmax classifier.

4. Results

As stated earlier, we have evaluated the proposed unified attention network on standard datasets for image-based camera localization and indoor scene classification. We discuss these datasets later in Sec. 4.2.

4.1. Practical considerations

We used *TensorFlow* framework [1] to implement and train our models. Every model was trained end-to-end using ADAM [22] optimizer with the parameters: $\beta_1 = 0.9$, $\beta_2 = 0.999$, and $\epsilon = 1 \times 10^{-8}$. We used a learning rate equal to 1×10^{-4} . The regularization parameter, $\lambda = 2 \times 10^{-4}$, was added to weights, but not to biases. The dropout probability was set to 0.5 for all the experiments.

Dataset	PoseNet [21]	Bayesian PoseNet [18]	LSTM PoseNet [37]	Ours				
				Time Step-1	Time Step-2	Time Step-3	Time Step-4	Improvement (meter, degree) %
Kings College	1.66 m, 4.86°	1.74 m, 4.06°	0.99 m, 3.65°	0.82 m, 3.07°	0.79 m, 3.02°	0.78 m, 3.01°	0.78 m, 2.99°	+21, +18
Old Hospital	2.62 m, 4.90°	2.57 m, 5.14°	1.51 m, 4.29°	1.51 m, 4.42°	1.42 m, 4.59°	1.48 m, 4.33°	1.39 m, 4.23°	+7, +1
Shop Facade	1.41 m, 7.18°	1.25 m, 7.54°	1.18 m, 7.44°	0.97 m, 5.99°	0.96 m, 5.98°	0.91 m, 6.02°	0.93 m, 5.92°	+22, +20
St. Marys Church	2.45 m, 7.96°	2.11 m, 8.38°	1.52 m, 6.68°	1.44 m, 6.66°	1.40 m, 6.58°	1.42 m, 6.62°	1.43 m, 6.50°	+7, +2
Cambridge Landmarks Ave.	2.08 m, 6.83°	1.92 m, 6.28°	1.30 m, 5.52°	1.18 m, 5.03°	1.14 m, 5.04°	1.14 m, 4.99°	1.13 m, 4.91°	+13, +11
Chess	0.32 m, 6.08°	0.37 m, 7.24°	0.24 m, 5.77°	0.17 m, 5.49°	0.16 m, 5.49°	0.16 m, 5.46°	0.16 m, 5.47°	+33, +5
Fire	0.47 m, 14.0°	0.43 m, 13.7°	0.34 m, 11.9°	0.31 m, 11.7°	0.30 m, 11.6°	0.29 m, 11.6°	0.29 m, 11.6°	+14, +2
Heads	0.30 m, 12.2°	0.31 m, 12.0°	0.21 m, 13.7°	0.19 m, 14.7°	0.19 m, 14.4°	0.18 m, 14.3°	0.19 m, 14.1°	+14, -2
Office	0.48 m, 7.24°	0.48 m, 8.04°	0.30 m, 8.08°	0.31 m, 7.59°	0.29 m, 7.32°	0.28 m, 7.29°	0.28 m, 7.35°	+7, +9
Pumpkin	0.49 m, 8.12°	0.61 m, 7.08°	0.33 m, 7.00°	0.25 m, 6.42°	0.25 m, 6.31°	0.25 m, 6.32°	0.25 m, 6.29°	+24, +10
Red Kitchen	0.58 m, 8.31°	0.58 m, 7.51°	0.37 m, 8.83°	0.42 m, 8.06°	0.40 m, 7.88°	0.39 m, 7.89°	0.39 m, 7.96°	-5, +10
Stairs	0.48 m, 13.1°	0.48 m, 13.1°	0.40 m, 13.7°	0.38 m, 12.6°	0.39 m, 12.5°	0.39 m, 12.5°	0.39 m, 12.5°	+5, +8
7-Scenes Ave.	0.44 m, 9.01°	0.46 m, 9.81°	0.31 m, 9.85°	0.29 m, 9.50°	0.29 m, 9.35°	0.27 m, 9.33°	0.27 m, 9.32°	+12, +5
TUM-LSI	1.87 m, 6.14°	-	1.31 m, 2.79°	1.13 m, 3.60°	1.00 m, 3.27°	1.01 m, 3.38°	1.01 m, 3.17°	+16, -13

Table 3: Camera localization results. Median localization error achieved by the proposed unified attention model over four time steps on camera pose estimation datasets: Cambridge Landmarks, 7-Scenes, and TUM-LSI dataset. Our method achieves lower errors in almost every case. LSTM PoseNet method [37] posts lower errors for Red Kitchen scene in the 7-Scenes dataset. Bold values indicate the lowest error achieved for each row.

Dataset	CNNaug- SVM [32]	S ² ICA [9]	GoogleNet [34]	Ours				
				Time Step-1	Time Step-2	Time Step-3	Time Step-4	Improvement (%)
MIT-67	69.0 %	71.2 %	67.2 %	74.3 %	75.1 %	75.0%	74.2 %	+5.4

Table 4: Scene classification results. Mean accuracy results on MIT-67 indoor dataset for the proposed unified attention network. The proposed method achieves higher accuracy compared to competing methods. The highest accuracy is shown in boldface.

For indoor scene classification task, we resized the images to 256×256 . During training, we performed random crops of 224×224 pixels. At test time, we performed centered crop of 224×224 pixels. The batch size was set to 20. The images were mean subtracted per channel.

For camera pose estimation, we resized the images to 256×455 pixels. During training, we performed random crops of 224×224 pixels. At test time, we performed center crop of 224×224 pixels. The batch size was set to 16. Similar to [21] and [37], separate mean images were computed for each channel and the images were mean subtracted per channel. For Cambridge Landmarks dataset β value was set between 250 to 2000. For 7-Scenes dataset β value was set between 120 to 750, and for TUM-LSI dataset β value was set to 1000.

For both camera pose estimation and indoor scene clas-

sification, we used the same pre-trained CNN layers as used by previous methods. Specifically, we used the original GoogLeNet weights trained on Places⁴ [44]. By necessity, we converted these provided trained network weights to be able to use these in *TensorFlow*.

4.2. Datasets

Cambridge Landmarks [21] A large scale outdoor dataset, containing five outdoor datasets. For our experiments, we only use the four datasets that were used by [21] and [37]. The dataset consists of RGB images. Six degrees-of-freedom camera poses are provided for each image. The dataset was collected using a smart phone, and structure from motion was employed to label each image with its cor-

⁴<http://places.csail.mit.edu/downloadCNN.html>

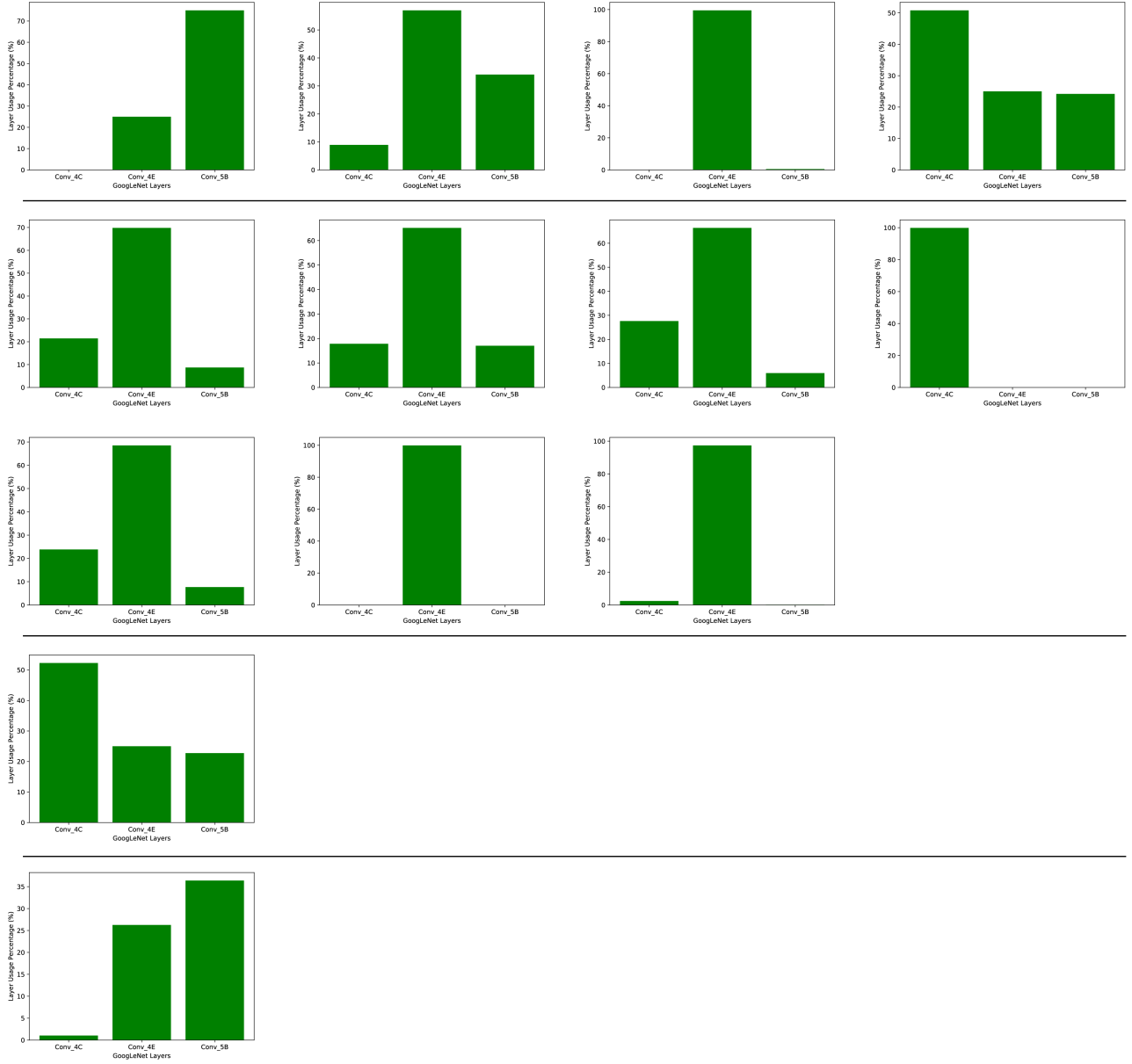


Figure 3: CNN Layer Selection Frequencies (LSF) for the four datasets. The top row contains LSF for the four scenes in Cambridge Landmarks datasets. The next two rows contain the seven scenes in the 7Scenes dataset. Fourth row represents LSF results for TUM-LSI. The last row represents layer selection for the MIT-67 dataset. Top four rows correspond to results on the camera pose estimation problem, and the bottom row show results for the scene classification problem. The horizontal bins refer to GoogLeNet layers Conv-4C, Conv-4E, and Conv-5B. The vertical axis represents layer usage percentages.

responding camera pose.

7-Scenes [33] A small scale indoor dataset, which consists of seven different scenes. These scenes were obtained using Kinect RGB-D camera, and KinectFusion[14] was used to obtain the ground truth. We use the train/test split used by [21] and [37]. Scene contain ambiguous regions, which makes camera localization difficult.

TU Munich Large-Scale Indoor (TUM-LSI) [37] An indoor dataset, which covers an area of two orders of magnitude larger than that covered by the 7Scenes dataset. It consists of 875 training images and 220 testing images. We use the train/test split used by [37]. This is a challenging dataset to localize due to repeated structural elements with nearly identical appearance.

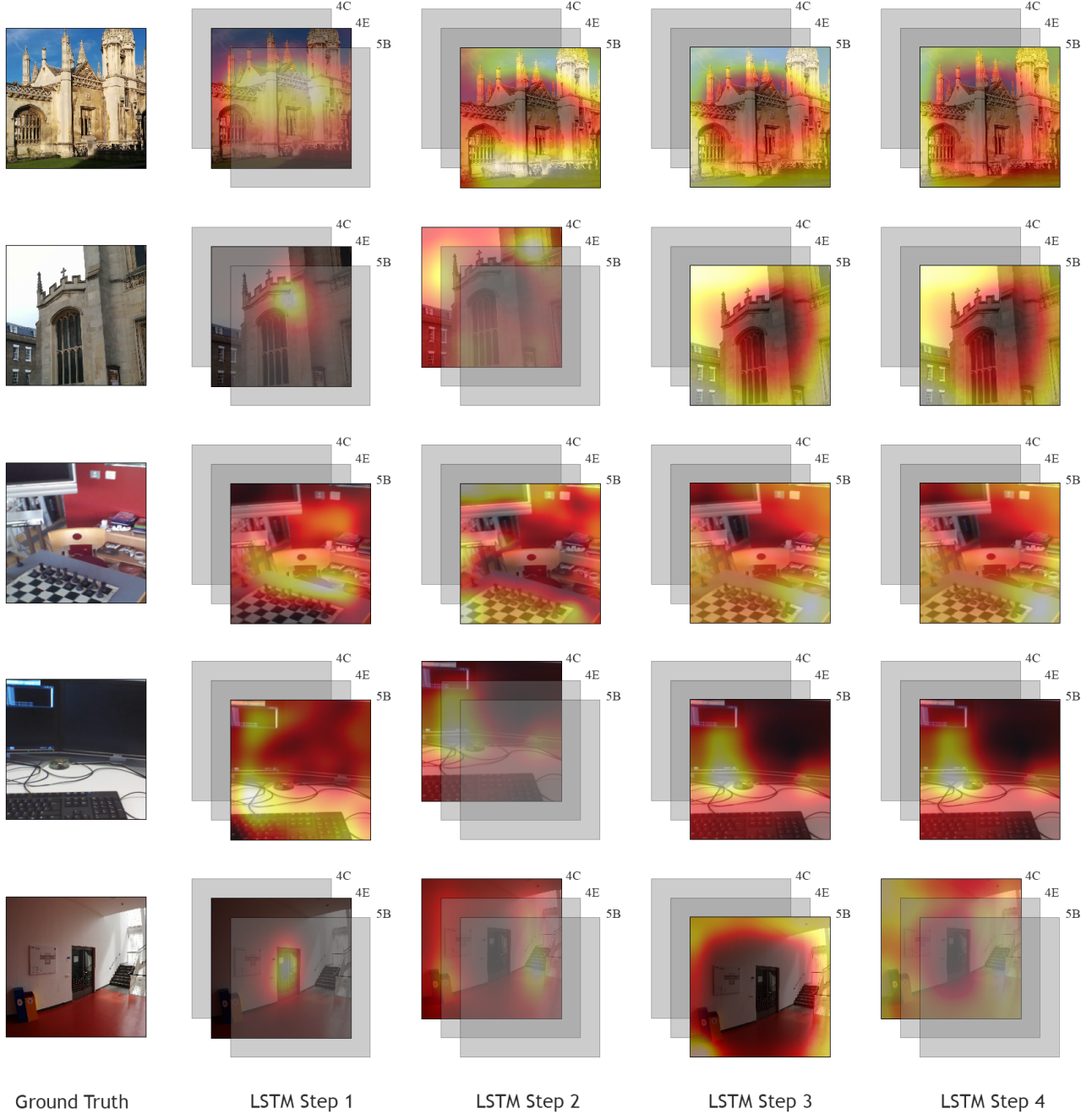


Figure 4: Unified Attention Network in action. (Left) input image and (Right columns) visualization of “what” and “where” aspects of attention.

MIT-67 indoor scenes [30] Images taken primarily in four different indoor environments—store, home, public spaces, leisure and working places. The dataset contains 67 categories in total. We used the official train/test split provided by [30]. Each category has 80 training images and 20 testing images.

5. Discussion

To see if layer selection combined with spatial soft attention helps, we manually selected feature maps from GoogLeNet layers Conv-4E, Conv-4D, and Conv-4C and compare the network performance against that obtained when using feature maps from GoogLeNet. In a typical setting feature maps from GoogLeNet layer Conv-5B would

be used.

Table 1 shows the results of this exercise on camera pose estimation task. Median localization errors improve for both Old Hospital and Office datasets when we use CNN layers other than Conv-5B. In the case of TUM-LSI, we notice that best localization performance is achieved when using CNN layer Conv-5B.

Table 2 shows the results of the similar exercise on indoor scene classification. It includes results for six out of 67 indoor scene classes.⁵ Here too we notice a trend. The mean classification accuracy for Auditorium, Children Room, Garage, Laboratory Wet, and Shoe Shop categories improve as we select layers other than Conv-5B. Conv-5B achieves the best results for Concert Hall.

These results suggest that the “correct” CNN layer is data and task dependent. An attention mechanism that learns a policy to probe different layers can exploit this fact and achieve better performance.

5.1. Evaluation

Camera localization Table 3 compares the proposed method against recent, previous image-based camera pose estimation methods [21, 18, 37]. For our method, we show localization errors—both, position (in meters) and orientation (in degrees)—at steps one to four for the attention LSTM, which controls both soft- and hard-attention, i.e., at each step, UAN decides “what” to look at, and “where” to look at. The lowest errors in each row are shown in bold-face. Our method achieves better performance in the majority of cases. The notable exceptions are: PoseNet does a better at estimating orientation for Heads scene and position for Red Kitchen scene in the 7-Scenes dataset.

For these results the layer selection mechanism selects one of the following three GoogLeNet layers at each time step: Conv-4C, Conv-4E, and Conv-5B. Figure 3 plots the layer selection percentages for each dataset. These plots suggest that different layers are indeed selected during inference. Meaning the network is attending to different layers as it attempts to regress the position and orientation of the camera.

Indoor scene classification Table 4 compares the proposed method against four competing methods [32, 9, 34]. Again, for our method, we show classification accuracies in percentages at steps one to four for the attention LSTM deciding “what” to look at and “where” to look at. Our method achieves the highest classification accuracy, posting an improvement of over five percent over the scheme proposed in [9]. The last row of Fig. 3 plot layer selection frequencies at inference times. The layer selection mechanism selects one of the following three GoogLeNet layers at each time step: Conv-4C, Conv-4E, and Conv-5B. This confirms

⁵We provide more examples in supplementary material.

our understanding that the network indeed attends to different layers as it attempts to classify an image.

6. Limitations and Future work

The network selection is blindly learned through data. Using Gumbel-Softmax trick helps to sample in a differentiable fashion but also increases the stochasticity in the learning process. Therefore the network may not converge to the best optimal layer. Figures 7 and 10 show that taking more steps does not necessarily lead to better performance. For future work, it would be interesting to investigate how to inject prior information or semantic information into the network. In this manner taking more steps actually improves/stabilizes the result and network can have a better chance of looking at the best optimal layers.

7. Conclusion

We propose a new architecture, referred to as UAN, that learns to attend to different Convolutional Neural Networks (CNN) layers (i.e., different levels of abstraction) and different spatial locations (i.e., specific layers within a given feature map) in a sequential manner to perform the task at hand. This architecture combines the “what” and the “where” aspects of attention, i.e., “what” level of abstraction to attend to, and “where” should the network look at. Fig. 4 illustrates layer selection and spatial soft attention at different LSTM steps for a small set of input images.

We demonstrate UAN over two computer vision tasks: image-based camera localization and indoor scene classification. For image-based camera localization we compare our work with previous approaches proposed in [21] and [37] on 7-Scenes, Cambridge landmarks, and TUM-LSI datasets. For indoor scene classification, we compare UAN with existing approaches proposed in [32] and [9] on MIT-67 indoor scene dataset. We show empirically that UAN improves upon results of previous approaches. In the future, we intend to apply this model to other computer vision tasks.

8. Acknowledgments

The authors would like to thank Kamyar Nazeri (Imaging lab, University of Ontario Institute of Technology, Canada) for providing support on figures presented in this paper. We gratefully acknowledge the support of NVIDIA Corporation with the donation of the Titan Xp GPU used for this research.

References

- [1] M. Abadi, P. Barham, J. Chen, Z. Chen, A. Davis, J. Dean, M. Devin, S. Ghemawat, G. Irving, M. Isard, et al. Tensorflow: a system for large-scale machine learning. In *OSDI*, volume 16, pages 265–283, 2016.

- [2] R. Anati, D. Scaramuzza, K. G. Derpanis, and K. Daniilidis. Robot localization using soft object detection. pages 4992–4999, 2012.
- [3] J. Ba, V. Mnih, and K. Kavukcuoglu. Multiple object recognition with visual attention. volume abs/1412.7755, 2014.
- [4] V. Balntas, S. Li, and V. Prisacariu. Relocnet: Continuous metric learning relocalisation using neural nets. In *Proceedings of the European Conference on Computer Vision (ECCV)*, pages 751–767, 2018.
- [5] E. Brachmann and C. Rother. Learning less is more-6d camera localization via 3d surface regression. In *Proc. CVPR*, volume 8, 2018.
- [6] C. Doersch, A. Gupta, and A. A. Efros. Mid-level visual element discovery as discriminative mode seeking. In *Advances in neural information processing systems*, pages 494–502, 2013.
- [7] J. Donahue, L. A. Hendricks, M. Rohrbach, S. Venugopalan, S. Guadarrama, K. Saenko, and T. Darrell. Long-term recurrent convolutional networks for visual recognition and description. volume 39, pages 677–691, 2017.
- [8] C. Goller and A. Kuchler. Learning task-dependent distributed representations by backpropagation through structure. *Neural Networks*, 1:347–352, 1996.
- [9] M. Hayat, S. H. Khan, M. Bennamoun, and S. An. A spatial layout and scale invariant feature representation for indoor scene classification. volume 25, pages 4829–4841. IEEE, 2016.
- [10] K. He, G. Gkioxari, P. Dollár, and R. Girshick. Mask r-cnn. In *Computer Vision (ICCV), 2017 IEEE International Conference on*, pages 2980–2988. IEEE, 2017.
- [11] K. He, X. Zhang, S. Ren, and J. Sun. Deep residual learning for image recognition. In *The IEEE Conference on Computer Vision and Pattern Recognition (CVPR)*, June 2016.
- [12] S. Hochreiter and J. Schmidhuber. Long short-term memory. volume 9, pages 1735–1780, 1997.
- [13] E. Ilg, N. Mayer, T. Saikia, M. Keuper, A. Dosovitskiy, and T. Brox. FlowNet 2.0: Evolution of optical flow estimation with deep networks. In *IEEE conference on computer vision and pattern recognition (CVPR)*, volume 2, page 6, 2017.
- [14] S. Izadi, D. Kim, O. Hilliges, D. Molyneaux, R. Newcombe, P. Kohli, J. Shotton, S. Hodges, D. Freeman, A. Davison, et al. Kinectfusion: real-time 3d reconstruction and interaction using a moving depth camera. In *Proceedings of the 24th annual ACM symposium on User interface software and technology*, pages 559–568. ACM, 2011.
- [15] E. Jang, S. Gu, and B. Poole. Categorical reparameterization with gumbel-softmax. 2017.
- [16] D. Jayaraman and K. Grauman. Learning to look around. volume abs/1709.00507, 2017.
- [17] M. Juneja, A. Vedaldi, C. Jawahar, and A. Zisserman. Blocks that shout: Distinctive parts for scene classification. In *Proceedings of the IEEE Conference on Computer Vision and Pattern Recognition*, pages 923–930, 2013.
- [18] A. Kendall and R. Cipolla. Modelling uncertainty in deep learning for camera relocalization. pages 4762–4769, 2016.
- [19] A. Kendall, R. Cipolla, et al. Geometric loss functions for camera pose regression with deep learning. In *Proc. CVPR*, volume 3, page 8, 2017.
- [20] A. Kendall and Y. Gal. What uncertainties do we need in bayesian deep learning for computer vision? In *Advances in neural information processing systems*, pages 5574–5584, 2017.
- [21] A. Kendall, M. Grimes, and R. Cipolla. PoseNet: A convolutional network for real-time 6-dof camera relocalization. pages 2938–2946, 2015.
- [22] D. P. Kingma and J. Ba. Adam: A method for stochastic optimization. 2014.
- [23] A. Krizhevsky, I. Sutskever, and G. E. Hinton. ImageNet classification with deep convolutional neural networks. In *Advances in neural information processing systems*, pages 1097–1105, 2012.
- [24] H. Larochelle and G. E. Hinton. Learning to combine foveal glimpses with a third-order boltzmann machine. In *Advances in neural information processing systems*, pages 1243–1251, 2010.
- [25] Y. LeCun, B. E. Boser, J. S. Denker, D. Henderson, R. E. Howard, W. E. Hubbard, and L. D. Jackel. Handwritten digit recognition with a back-propagation network. In *Advances in neural information processing systems*, pages 396–404, 1990.
- [26] C. Ledig, L. Theis, F. Huszár, J. Caballero, A. Cunningham, A. Acosta, A. P. Aitken, A. Tejani, J. Totz, Z. Wang, et al. Photo-realistic single image super-resolution using a generative adversarial network. In *CVPR*, volume 2, page 4, 2017.
- [27] C. J. Maddison, D. Tarlow, and T. Minka. A* sampling. In *Advances in Neural Information Processing Systems*, pages 3086–3094, 2014.
- [28] V. Mnih, N. Heess, A. Graves, and K. Kavukcuoglu. Recurrent models of visual attention. pages 2204–2212, 2014.
- [29] T. Ngo and B. Manjunath. Saccade gaze prediction using a recurrent neural network. 2017.
- [30] A. Quattoni and A. Torralba. Recognizing indoor scenes. In *2009 IEEE Conference on Computer Vision and Pattern Recognition*, pages 413–420. IEEE, 2009.
- [31] T. Sattler, B. Leibe, and L. Kobbelt. Efficient & effective prioritized matching for large-scale image-based localization. volume 39, pages 1744–1756, 2017.
- [32] A. Sharif Razavian, H. Azizpour, J. Sullivan, and S. Carlsson. Cnn features off-the-shelf: an astounding baseline for recognition. In *Proceedings of the IEEE conference on computer vision and pattern recognition workshops*, pages 806–813, 2014.
- [33] J. Shotton, B. Glocker, C. Zach, S. Izadi, A. Criminisi, and A. Fitzgibbon. Scene coordinate regression forests for camera relocalization in rgb-d images. In *Proceedings of the IEEE Conference on Computer Vision and Pattern Recognition*, pages 2930–2937, 2013.
- [34] C. Szegedy, W. Liu, Y. Jia, P. Sermanet, S. E. Reed, D. Anguelov, D. Erhan, V. Vanhoucke, and A. Rabinovich. Going deeper with convolutions. pages 1–9, 2015.
- [35] Y. Tang, N. Srivastava, and R. R. Salakhutdinov. Learning generative models with visual attention. In *Advances in Neural Information Processing Systems*, pages 1808–1816, 2014.

- [36] A. Veit and S. Belongie. Convolutional networks with adaptive inference graphs. In *European Conference on Computer Vision*, pages 3–18. Springer, 2018.
- [37] F. Walch, C. Hazirbas, L. Leal-Taixé, T. Sattler, S. Hilsenbeck, and D. Cremers. Image-based localization using lstms for structured feature correlation. pages 627–637, 2017.
- [38] L. Wang, T. Liu, G. Wang, K. L. Chan, and Q. Yang. Video tracking using learned hierarchical features. volume 24, pages 1424–1435. IEEE, 2015.
- [39] T. Weyand, I. Kostrikov, and J. Philbin. Planet - photo geolocation with convolutional neural networks. pages 37–55, 2016.
- [40] S. Xingjian, Z. Chen, H. Wang, D.-Y. Yeung, W.-K. Wong, and W.-c. Woo. Convolutional lstm network: A machine learning approach for precipitation nowcasting. In *Advances in neural information processing systems*, pages 802–810, 2015.
- [41] K. Xu, J. Ba, R. Kiros, K. Cho, A. C. Courville, R. Salakhutdinov, R. S. Zemel, and Y. Bengio. Show, attend and tell: Neural image caption generation with visual attention. pages 2048–2057, 2015.
- [42] W. Zaremba, I. Sutskever, and O. Vinyals. Recurrent neural network regularization. 2014.
- [43] M. D. Zeiler and R. Fergus. Visualizing and understanding convolutional networks. In *European conference on computer vision*, pages 818–833. Springer, 2014.
- [44] B. Zhou, A. Lapedriza, J. Xiao, A. Torralba, and A. Oliva. Learning deep features for scene recognition using places database. In *Advances in neural information processing systems*, pages 487–495, 2014.

A. Supplementary Materials

A.1. Detailed UAN Architecture

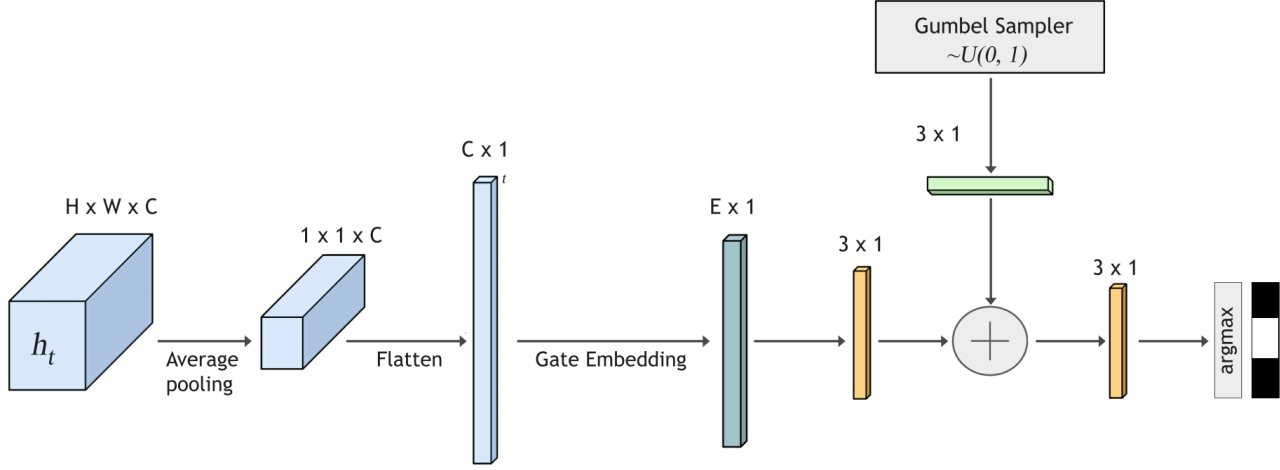


Figure 5: Layer Selection Mechanism.

Figure 5, illustrates the layer selection mechanism. The mechanism receives input h_t from ConvLSTM. It then performs an average pool and an intermediate gate embedding before prediction. We add the Gumbel samples to the predicted logits and perform an *argmax* to select the optimal layer. The gate embedding layer dimension E is much smaller than C . This gate embedding layer helps build a possible representation of incoming features at every LSTM steps, without significantly increasing the network parameters.

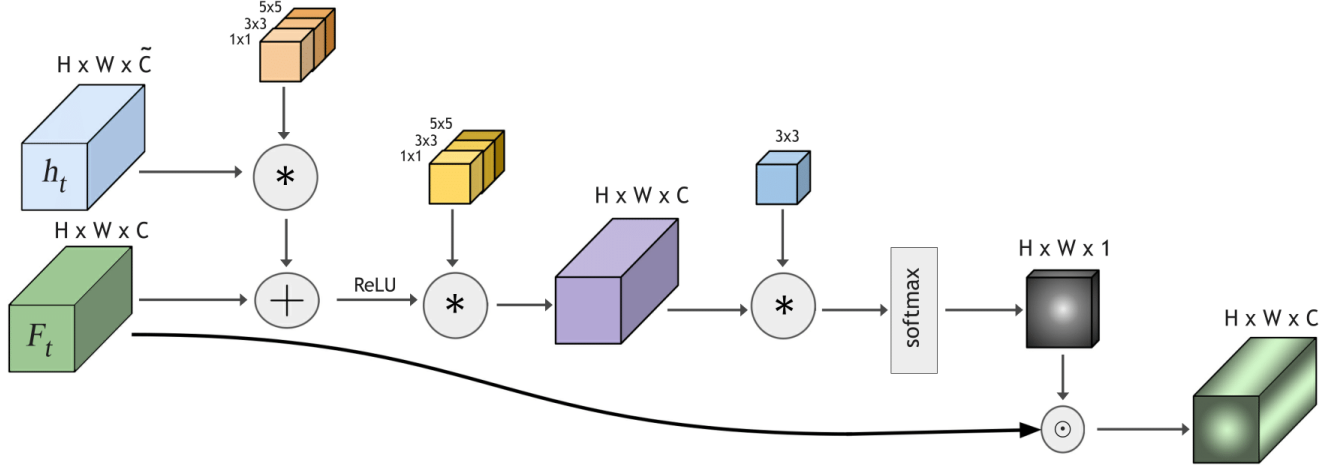


Figure 6: Soft Attention Mechanism.

Figure 6, illustrates the soft attention mechanism. Unlike the soft attention mechanism proposed in Xu *et al.* [41] ours replace fully-connected layers with convolutional layers (see Section A.2 for details). Specifically, we used multi-convolutional layers that uses different kernel sizes similar to an inception module. At each time step t , the module receives h_t from ConvLSTM and the selected feature layer F_t . The ConvLSTMs hidden state h_t is first converted to the appropriate channel size of the feature map. We add the embedding h_t and feature layer F_t . Then we apply a non-linearity (Leaky ReLU). After which we compute the attention weights and apply softmax to get the attention map. Then an element-wise multiplication is

Dataset	PoseNet [21]	LSTM PoseNet [37]	Ours				
			Time Step-1	Time Step-2	Time Step-3	Time Step-4	Improvement (meter, degree) %
Kings College	1.66 m, 4.86°	0.99 m , 3.65°	1.51 m, 2.57°	1.38 m, 2.64°	1.39 m, 2.63°	1.36 m, 2.63°	-27.2, +27.6
Old Hospital	2.62 m, 4.90°	1.51 m , 4.29°	3.82 m, 4.24°	3.67 m, 4.25°	3.72 m, 4.24°	3.33 m, 3.99°	-120.5, +6.9
Shop Facade	1.41 m, 7.18°	1.18 m, 7.44°	1.03 m, 4.75°	1.03 m, 4.57°	1.03 m, 4.50°	1.04 m, 4.52°	+12.7, +38.5
St. Marys Church	2.49 m, 6.17°	1.52 m , 6.68°	2.49 m, 6.17°	2.52 m, 6.14°	2.50 m, 6.21°	2.51 m, 6.20°	-63.8, +8
Cambridge Landmarks Ave.	2.08 m, 6.83°	1.30 m , 5.52°	2.21 m, 4.38°	2.15 m, 4.44°	2.16 m, 4.42°	2.06 m, 4.33°	-66.7, +21.5
Chess	0.32 m, 6.08°	0.24 m , 5.77°	0.29 m, 5.51°	0.28 m, 5.45°	0.29 m, 5.49°	0.29 m, 5.47°	-20.8, +5.5
Fire	0.47 m, 14.0°	0.34 m , 11.9°	0.49 m, 12.0°	0.49 m, 11.9°	0.50 m, 11.9°	0.50 m, 11.8°	-44.1, +0.8
Heads	0.30 m, 12.2°	0.21 m , 13.7°	0.26 m, 14.1°	0.26 m, 14.4°	0.27 m, 14.1°	0.27 m, 14.0°	-23.8, -2.1
Office	0.48 m, 7.24°	0.30 m , 8.08°	0.61 m, 7.85°	0.62 m, 7.82°	0.64 m, 7.89°	0.64 m, 7.88°	-103.3, +3.2
Pumpkin	0.49 m, 8.12°	0.33 m , 7.00°	0.53 m, 6.99°	0.52 m, 7.01°	0.51 m, 7.13°	0.51 m, 7.22°	-54.5, +0.1
Red Kitchen	0.58 m, 8.31°	0.37 m , 8.83°	0.55 m, 8.67°	0.54 m, 8.63°	0.54 m, 8.67°	0.54 m, 8.78°	-45.0, +2.2
Stairs	0.48 m, 13.1°	0.40 m , 13.7°	0.46 m, 12.8°	0.48 m, 12.8°	0.48 m, 12.8°	0.49 m, 12.9°	-15.0, +6.5
7-Scenes Ave.	0.44 m, 9.01°	0.31 m , 9.85°	0.45 m, 9.70°	0.45 m, 9.71°	0.46 m, 9.71°	0.46 m, 9.72°	-45.1, +1.5
TUM-LSI	1.87 m, 6.14°	1.31 m , 2.79°	4.20 m, 1.87°	3.93 m, 2.14°	3.93 m, 2.15°	4.10 m, 2.99°	+16, +32

Table 5: Median localization error achieved by the convolutional attention model over four time steps on camera pose estimation datasets: Cambridge Landmarks, 7-Scenes, and TUM-LSI dataset. Bold values indicate the lowest error achieved for each row.

performed between features and attention map to get the final output of the soft attention module. The Multi-ConvLSTM is applied to attention output. At each time step the LSTM output is used for prediction.

A.2. Multi-Convolutional Approach

In this section, we describe our motivation for using the multi-convolutional approach. To showcase how we arrived at the proposed approach, we provide evaluation on all three datasets for the pose estimation. We initially started with the same implementation as Xu *et al.* [41] for soft attention, by using fully connected layers. The model ended up overfitting the data and showed poor performance on the test set. Also, the network converged to select only a single spatial feature instead of probing through the other spatial features at different LSTM time-steps. Our first solution was converting fully connected layers into fully convolutional layers. The results for this approach on pose estimation is shown in Table 5. The results shown is quite far from [37] especially on the position, but interestingly error was close to [21].

We found that our model was underfitting the training data. Naively increasing the depth size or kernel size was not showing any significant improvements. Therefore by taking inspiration from the inception module proposed in GoogLeNet [34], we converted each convolutional layer into multi-convolutional layers. We used three convolutional kernels with kernel sizes of 1x1, 3x3 & 5x5 and stacked their final output together. Similarly, in the case of ConvLSTM, we used four convolutional kernels with kernel sizes of 1x1, 3x3, 5x5 & 7x7. Then stacked their final output together for prediction. This approach helped improve results significantly as shown in Table 6. After which we applied our contribution of layer selection mechanism to form UAN. The Final UAN results for pose estimation is shown in Table 3 in the main paper.

Dataset	PoseNet [21]	LSTM PoseNet [37]	Ours				
			Time Step-1	Time Step-2	Time Step-3	Time Step-4	Improvement (meter, degree) %
Kings College	1.66 m, 4.86°	0.99 m, 3.65°	0.91 m , 3.96°	0.94 m, 4.15°	0.95 m, 4.11°	0.95 m, 4.02°	+8.0, -8.4
Old Hospital	2.31 m, 5.38°	1.51 m , 4.29°	3.40 m, 4.22°	3.19 m, 4.26°	3.05 m, 4.38°	3.04 m, 4.30°	-101.0, +1.6
Shop Facade	1.41 m , 7.18°	1.18 m, 7.44°	0.91 m , 5.90°	1.00 m, 5.86°	0.95 m, 5.80°	0.93 m, 5.76°	+22.8, +22.5
St Marys Church	2.65 m, 8.48°	1.52 m , 6.68°	1.65 m, 6.91°	1.64 m, 7.04°	1.64 m, 7.07°	1.63 m, 7.11°	-7.2, -3.4
Cambridge Landmarks Ave.	2.08 m, 6.83°	1.30 m , 5.52°	1.71 m, 5.24°	1.69 m, 5.32°	1.64 m, 5.34°	1.63 m, 5.29°	-25.3, +5.0
Chess	0.32 m, 6.60°	0.24 m, 5.77°	0.16 m , 6.60°	0.16 m, 6.60°	0.16 m, 6.55°	0.16 m , 6.53°	+33.3, +5.5
Fire	0.47 m, 14.0°	0.34 m, 11.9°	0.34 m, 11.6°	0.32 m, 11.7°	0.32 m , 11.7°	0.32 m, 11.7°	+5.8, +2.5
Heads	0.30 m, 12.2°	0.21 m, 13.7°	0.19 m, 12.8°	0.18 m , 12.8°	0.18 m, 12.8°	0.18 m, 12.8°	+14.2, +6.5
Office	0.48 m, 7.24°	0.30 m , 8.08°	0.44 m, 8.13°	0.42 m, 8.03°	0.41 m, 7.97°	0.41 m, 7.96°	-36.6, +1.4
Pumpkin	0.49 m, 8.12°	0.33 m, 7.00°	0.28 m, 6.14°	0.28 m, 6.15°	0.28 m , 6.15°	0.28 m, 6.19°	+15.1, +12.2
Red Kitchen	0.58 m, 8.34°	0.37 m , 8.83°	0.42 m, 8.63°	0.42 m, 8.79°	0.42 m, 8.63°	0.42 m, 8.81°	-13.5, +2.2
Stairs	0.48 m, 13.1°	0.40 m, 13.7°	0.32 m , 12.4°	0.33 m, 12.5°	0.32 m, 12.7°	0.32 m, 12.8°	+20.0, 9.4
7-Scenes Ave.	0.44 m, 9.94°	0.31 m, 9.85°	0.30 m, 9.47°	0.30 m, 9.51°	0.29 m , 9.49°	0.29 m, 9.59°	+6.4, +3.6
TUM-LSI	1.87 m, 6.14°	1.31 m, 2.79°	1.27 m, 2.99°	1.17 m, 2.90°	1.21 m, 2.89°	1.15 m , 2.87°	+12.2, -2.8

Table 6: Median localization error achieved by the multi-convolutional attention model over four time steps on camera pose estimation datasets: Cambridge Landmarks, 7-Scenes, and TUM-LSI dataset. Bold values indicate the lowest error achieved for each row.

B. Visualization

In this section, we show the visualization of results along with how the results change when we take multiple steps.

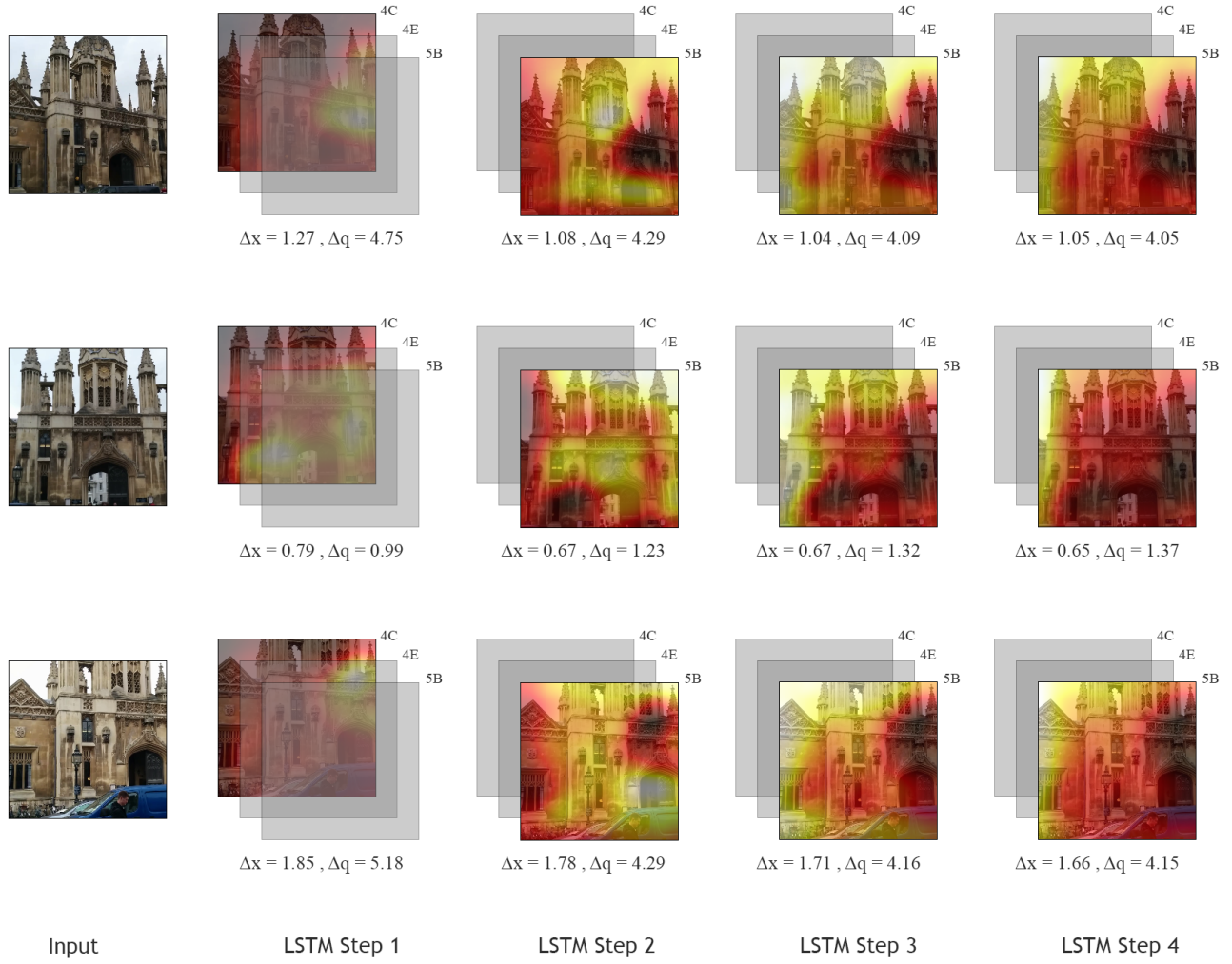


Figure 7: UAN Visualization on Kings College Dataset. At each LSTM step, position(Δx) and rotation(Δq) error with respect to ground truth is reported.

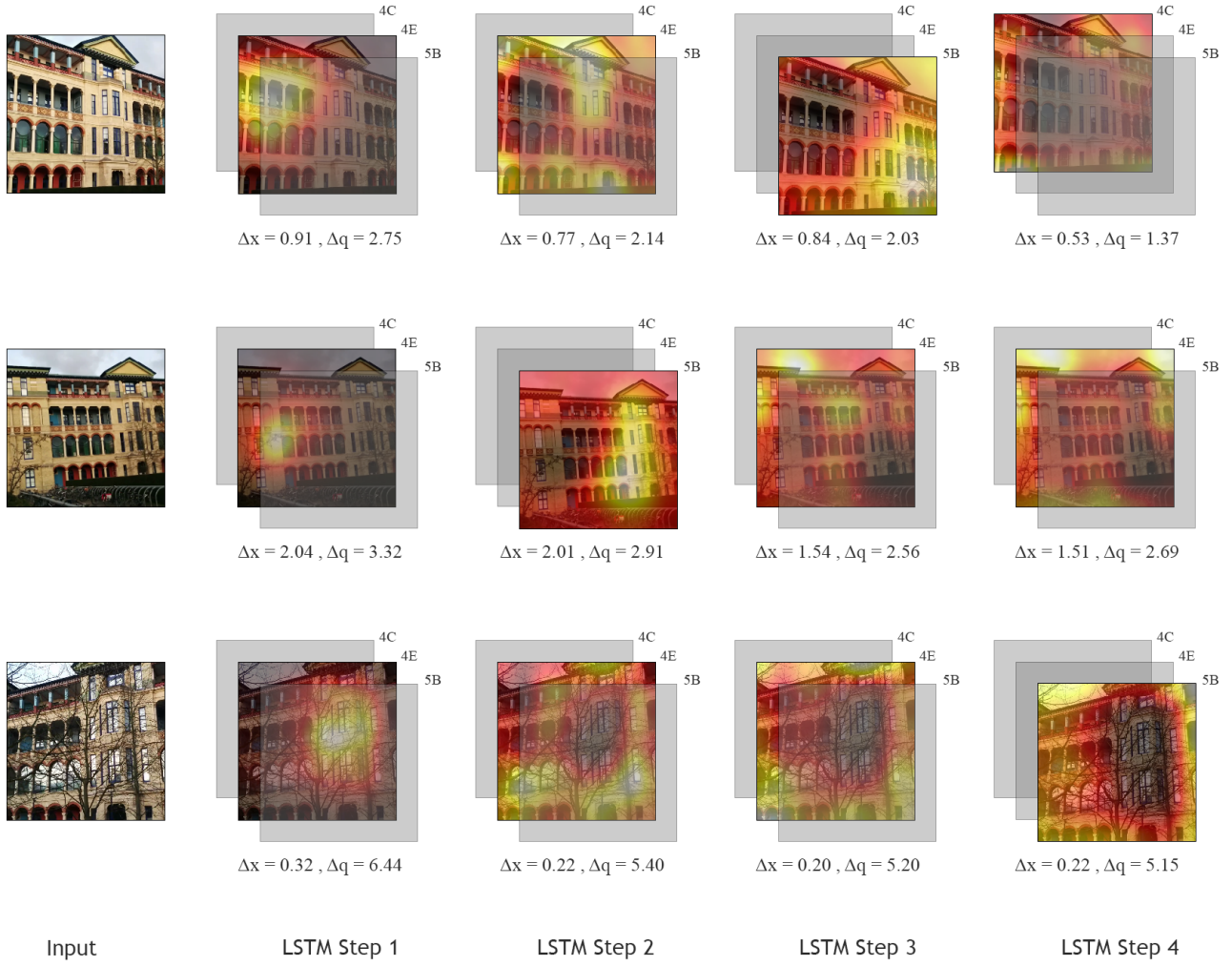


Figure 8: UAN Visualization on Old Hospital Dataset. At each LSTM step, position(Δx) and rotation(Δq) error with respect to ground truth is reported.

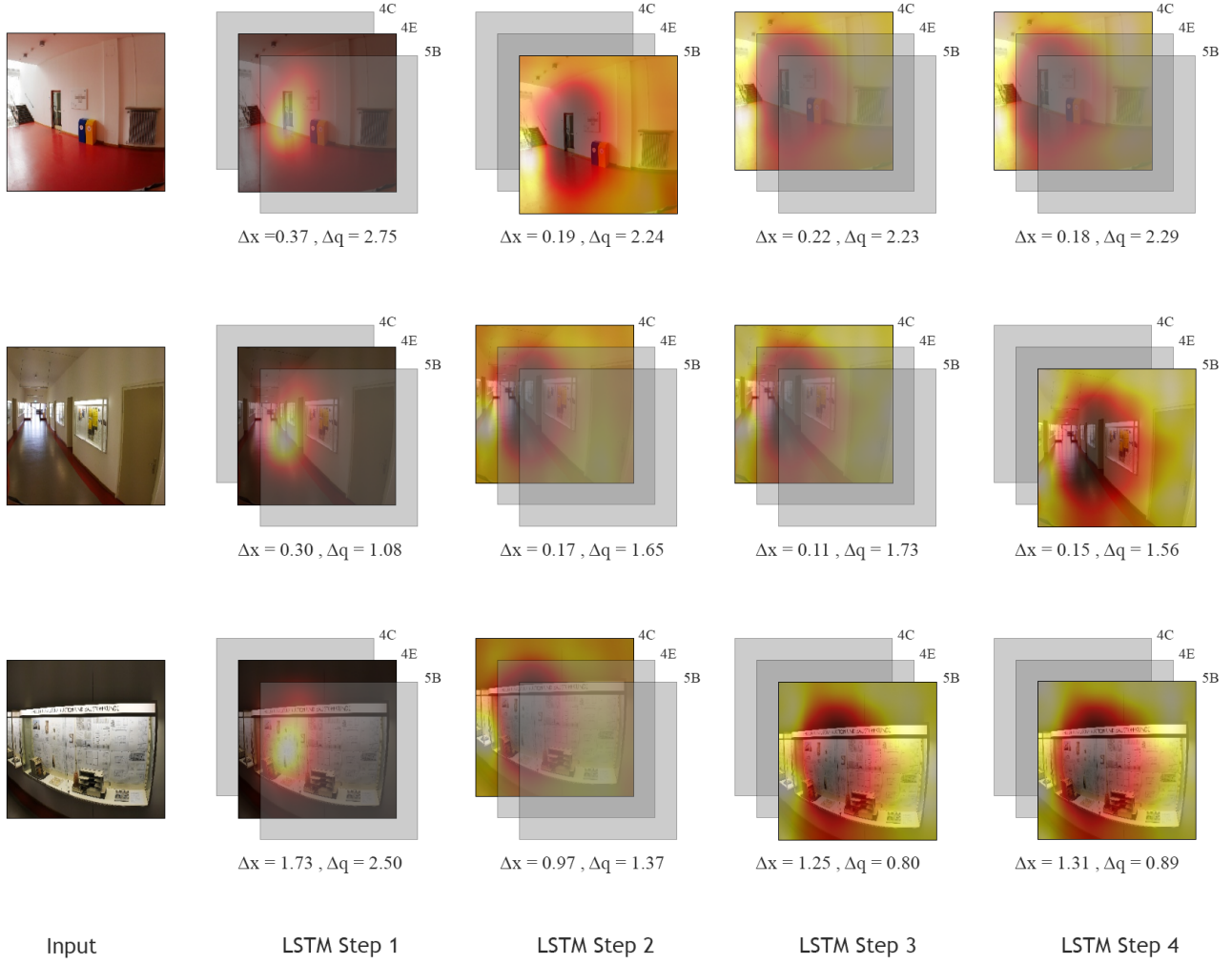


Figure 9: UAN Visualization on TUM-LSI Dataset. At each LSTM step, position(Δx) and rotation(Δq) error with respect to ground truth is reported.

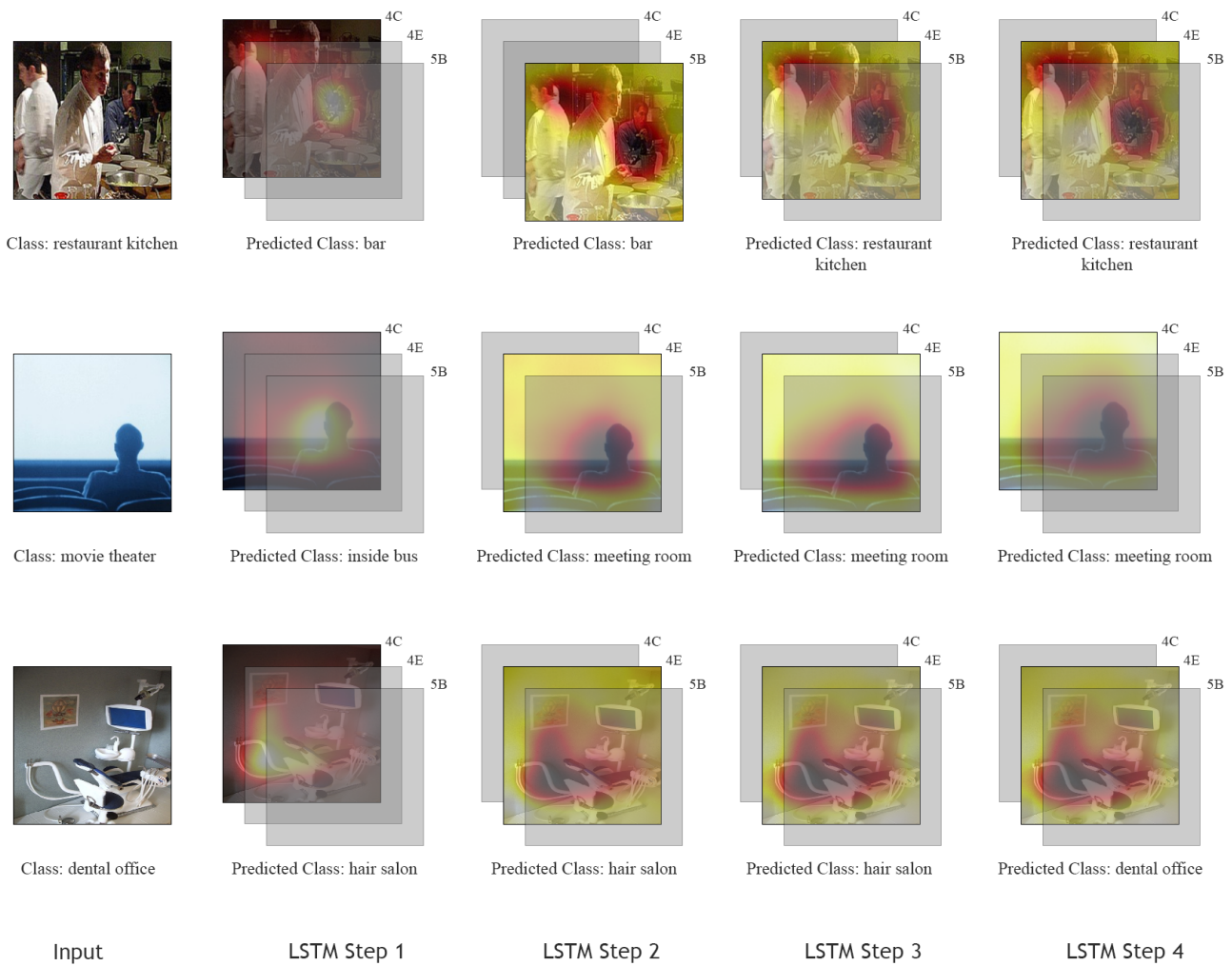


Figure 10: UAN Visualization on MIT-Indoor Scene dataset. At each LSTM step, the best prediction is reported.